Experiments with a hierarchical inverse dynamics controller on a torque-controlled humanoid

Alexander Herzog[1], Ludovic Righetti[1,2], Felix Grimminger[1], Peter Pastor[2] and Stefan Schaal[1,2]

***Abstract*— Recently several hierarchical inverse dynamics controllers based on quadratic programs have been proposed for application to torque controlled robots. They have important theoretical benefits but have never been implemented on a torque controlled robot where model inaccuracies and real-time computation requirements can be problematic. In this contribution we present experimental results for the control of the lower body of a humanoid robot using these algorithms. We propose a simplification of the optimization problem that allows us to decrease computation time enough to implement it in a fast torque control loop. Experiments demonstrate the applicability of the approach. In a first experiment, we implement a momentum-based balance controller which shows robust performance in face of unknown disturbances. In a second experiment, a tracking task is evaluated to demonstrate the performance of the controller with more complicated hierarchies. Our results show that hierarchical inverse dynamics controllers can be efficiently used for feedback control of humanoid robots and that momentum-based balance control can be efficiently implemented on a real robot.**

I. INTRODUCTION

We expect autonomous legged robots to perform complex tasks in constant interaction with an uncertain and changing environment (e.g. in a disaster relief scenario). Therefore, we need to design algorithms that can generate precise but compliant motions while optimizing the interactions with the environment. In this context, the choice of a control strategy for legged robots is of primary importance as it can drastically improve performance in face of unexpected disturbances and therefore open the way for agile robots, whether they are locomoting or performing manipulation tasks.

As robots with torque control capabilities are becoming increasingly available [1], [2], [3], [4], torque control algorithms are required to fully exploit such capabilities. Indeed, such algorithms often offer high performance for motion control while guaranteeing a certain level of compliance [3], [5], [6], [7]. In addition, they also allow for the direct control of contact interactions with the environment [1], [8], [9], which is required during operation in dynamic and uncertain environments.

This research was supported in part by National Science Foundation grants ECS-0326095, IIS-0535282, IIS-1017134, CNS-0619937, IIS-0917318, CBET-0922784, EECS-0926052, CNS-0960061, the DARPA program on Autonomous Robotic Manipulation, the Army Research Office, the Okawa Foundation, the ATR Computational Neuroscience Laboratories, and the Max-Planck-Society.

[1]Autonomous Motion Department, Max Planck Institute for Intelligent Systems, Tübingen, Germany. first.lastname@tuebingen.is.mpg.de

[2]CLMC Lab, University of Southern California, Los Angeles, USA.

Recent contributions have demonstrated the relevance of torque control approaches for humanoid robots, for example for balancing capabilities [10], [11], [4], [12]. All these approaches try to regulate the position of the center of mass (CoM) of the robot to ensure that the robot does not fall while ensuring that contact forces are physically admissible. We can essentially distinguish two approaches. Passivity-based approaches on humanoids were originally proposed in [10] and recently extended in [4]. They compute admissible contact forces and control commands under quasi-static assumptions. The great advantage of such approaches is that they do not require a precise dynamic model of the robot. Moreover, robustness is generically guaranteed due to the passivity property of the controllers. However, the quasi-static assumption does not allow to take into account very dynamic motions like side stepping. On the other hand, controllers based on the full dynamic model of the robot have also been successfully implemented on legged robots [1], [9], [12]. These methods essentially perform a form of inverse dynamics. The advantage of such approaches is that they are in theory well suited for very dynamic motions. However, the need for a precise dynamic model makes them harder to implement. Moreover, it is generally required to simplify the optimization process to meet time requirements of fast control loops (typically 1KHz or faster on modern torque controlled robots).

There have been recently very promising approaches for controlling hierarchies of tasks using the full dynamics of the robot [13], [6], [14]. These approaches are more general than approaches based on pseudo-inverses as they naturally allow the inclusion of arbitrary types of tasks including inequalities. The problems are formulated as quadratic programs to be solved. It has been argued that the computational complexity of such methods are too high to be implemented on fast real-time control loops and to the best of our knowledge no such methods has been implemented on a humanoid robot with torque control capabilities. In [14], the trajectories computed in simulation are replayed on a real robot using joint space position control but the method is not directly used for feedback control on the robot. It is worth mentioning that [1] recently successfully implemented a controller using the full dynamics of the robot and task hierarchies on a quadruped torque controlled robot. The approach is based on pseudo-inverses and not quadratic programs which make it potentially inefficient to handle inequalities.

In this contribution, we present experimental results of an inverse dynamics controller with task hierarchies on a torque controlled humanoid lower body based on the QP formulation of [13]. First we propose a simplification of the dynamic constraints that allow us to generally reduce the computational complexity of algorithms using inverse dynamics. It allows us to implement our controller in a 1KHz real-time control loop. We present two different experiments in order to demonstrate the applicability of the approach. In one experiment, we implement a momentum-based balance controller as originally proposed by [15] and further developed in [11] to take into account dynamic constraints. This experiment demonstrates the capabilities of such momentum-based balance controllers on a torque controlled robot. The second experiment is a tracking task, demonstrating that tracking accuracy in operational space can still be achieved. It is, to the best of our knowledge, the first demonstration of the applicability of the methods proposed in [13] or [6] as feedback controllers on torque controlled humanoids (i.e. without joint space PD control).

II. HIERARCHICAL INVERSE DYNAMICS

For our experiments we write hierarchical inverse dynamics controllers and use the solver proposed by [13] to perform real-time feedback control. In the following we give a short summary on how tasks can be formulated and revisit the original solver formulation. In Sect. II-C we then propose a simplification to reduce the complexity of the original formulation. The simplification is also applicable to other inverse dynamics formulations.

A. Modelling Assumptions and Problem Formulation

Assuming rigid-body dynamics, we can write the equations of motion of a robot as

$$\mathbf{M}(\mathbf{q})\ddot{\mathbf{q}} + \mathbf{N}(\mathbf{q}, \dot{\mathbf{q}}) = \mathbf{S}^T\boldsymbol{\tau} + \mathbf{J}_c^T\boldsymbol{\lambda} \tag{1}$$

where $\mathbf{q} = [\mathbf{q}_j^T, \mathbf{x}^T]^T$ denotes the configuration of the robot. $\mathbf{q}_j \in \mathbb{R}^n$ is the vector of joint positions and $\mathbf{x} \in \mathrm{SE}(3)$ denotes the position and orientation of a frame fixed to the robot with respect to an inertial frame (the floating base). $\mathbf{M}(\mathbf{q})$ is the inertia matrix, $\mathbf{N}(\mathbf{q}, \dot{\mathbf{q}})$ is the vector of all forces (Coriolis, centrifugal, gravity, friction, etc...), $\mathbf{S} = [\mathbf{I}_{n\times n}\mathbf{0}]$ represents the underactuation, $\mathbf{J}_c$ is the Jacobian of the contact constraints and $\boldsymbol{\lambda}$ are the generalized contact forces.

Endeffectors in contact need to stay stationary. We express the constraint that the feet (or hands) in contact with the environment do not move ($\mathbf{x}_c = \mathit{const}$) by differentiating it twice and using the fact that $\dot{\mathbf{x}}_c = \mathbf{J}_c\dot{\mathbf{q}}$. We get the following equality constraint

$$\mathbf{J}_c\ddot{\mathbf{q}} + \dot{\mathbf{J}}_c\dot{\mathbf{q}} = \mathbf{0}, \tag{2}$$

where $\mathbf{J}_c$ is the jacobian of the contact constraints.

For the dynamics to be consistent, the centers of pressure (CoPs) at the endeffectors need to reside in the interior of each endeffector support polygon. This can be expressed as a linear inequality by expressing the ground reaction force at the zero moment point. For the feet not to slip we constraint the GRFs to stay inside of the friction cones. In our case, we approximate the cones by pyramids to have linear inequality constraints. Especially important for generating control commands that are valid on a robot, is to take into account torque saturation limits $\boldsymbol{\tau}_{min} \leq \boldsymbol{\tau} \leq \boldsymbol{\tau}_{max}$. The same is true for joint limits, which can be written as $\ddot{\mathbf{q}}_{min} \leq \ddot{\mathbf{q}} \leq \ddot{\mathbf{q}}_{max}$, where $\ddot{\mathbf{q}}_{min}, \ddot{\mathbf{q}}_{max}$ are computed from the distance of $\mathbf{q}$ to the joint limits at each instant of time.

For the control objectives, each motion task can be expressed as $\ddot{\mathbf{x}}_{ref} = \mathbf{J}_x\ddot{\mathbf{q}} + \dot{\mathbf{J}}_x\dot{\mathbf{q}}$, where $\mathbf{J}_x$ is the task Jacobian and $\ddot{\mathbf{x}}_{ref}$ is a reference task acceleration (e.g. obtained from a PD-controller). Desired contact forces can be directly expressed as equalities on $\boldsymbol{\lambda}$. In general, we assume that each control objective can be expressed as a linear combination of $\ddot{\mathbf{q}}$, $\boldsymbol{\lambda}$ and $\boldsymbol{\tau}$.

At every control cycle, the equations of motion, Eq. (1), the constraints for physical consistency (torque saturation, CoP constraints, etc...) and our control objectives will all be expressed as affine equations of the variables $\ddot{\mathbf{q}}, \boldsymbol{\lambda}, \boldsymbol{\tau}$:

$$\mathbf{A}_i\mathbf{y} + \mathbf{a}_i \leq 0, \tag{3}$$

$$\mathbf{B}_i\mathbf{y} + \mathbf{b}_i = 0, \tag{4}$$

where $\mathbf{y} = [\ddot{\mathbf{q}}^T \ \boldsymbol{\lambda}^T \ \boldsymbol{\tau}^T]^T, \mathbf{A}_i \in \mathbb{R}^{m_i\times(2n+6+6c)}, \mathbf{a}_i \in \mathbb{R}^{m_i}, \mathbf{B}_i \in \mathbb{R}^{k_i\times(2n+6+6c)}, \mathbf{b}_i \in \mathbb{R}^{k_i}$ and $m_i, k_i, n, i \in \mathbb{N}$. $c \in \mathbb{N}$ is the number of constrained endeffectors.

The goal of the controller is to satisfy these objectives as well as possible. Each objective will have a different priority, with the highest priority in the hierarchy given to physical consistency. In a lower priority we will express balancing and motion tracking tasks and we will put tasks for redundancy resolution in the lowest priorities.

B. Hierarchical Inverse Dynamics Solver

The control objectives and constraints in Eqs. (3),(4) might not have a common solution, but need to be traded off against each other. In case of a push, for instance, the objective to decelerate the CoG might conflict with a swing foot task. A tradeoff can be expressed in form of slacks on the expressions in Eqs. (3),(4). The slacks then are minimized in a quadratic program

$$\min_{\mathbf{y},\mathbf{v},\mathbf{w}} \ \|\mathbf{v}\|^2 + \|\mathbf{w}\|^2 \tag{5}$$

$$\text{s.t.} \quad \mathbf{V}(\mathbf{A}\mathbf{y} + \mathbf{a}) \leq \mathbf{v}, \tag{6}$$

$$\mathbf{W}(\mathbf{B}\mathbf{y} + \mathbf{b}) = \mathbf{w}, \tag{7}$$

where $\mathbf{A}, \mathbf{B}, \mathbf{a}, \mathbf{b}$ are constructed from stacking $\mathbf{A}_i, \mathbf{B}_i, \mathbf{a}_i$ and $\mathbf{b}_i$ row-wise, e.g. $A^T = [\ldots \mathbf{A}_i^T \ \mathbf{A}_{i+1}^T \ldots]$. Matrices $\mathbf{V} \in \mathbb{R}^{(\sum m_i)\times(\sum m_i)}, \mathbf{W} \in \mathbb{R}^{(\sum k_i)\times(\sum k_i)}$ weigh the cost of constraints against each other and $\mathbf{v} \in \mathbb{R}^{\sum m_i}, \mathbf{w} \in \mathbb{R}^{\sum k_i}$ are slack variables.

Although, $\mathbf{W}, \mathbf{V}$ allow us to trade-off control objectives against each other, strict prioritization cannot be guaranteed with the formulation in Eq. (5). For instance, we might want to trade off tracking performance of tasks against each other, but we do not want to sacrifice physical consistency of a solution at any cost. In order to guarantee prioritization, we solve a sequence of QPs, where a QP with lower priority tasks is optimized over the set of optimal solutions of higher priority tasks as suggested by [13]. Given one solution

$(\mathbf{y}_r^*, \mathbf{v}_r^*)$ for the QP of priority r, all remaining optimal solutions $\mathbf{y}$ in that QP are expressed by the equations

$$\mathbf{y} = \mathbf{y}_r^* + \mathbf{Z}_r \mathbf{u}_{r+1}, \tag{8}$$
$$\mathbf{V}_r(\mathbf{A}_r \mathbf{y} + \mathbf{a}_r) - \mathbf{v}_r^* \leq 0, \tag{9}$$
$$\vdots$$
$$\mathbf{V}_1(\mathbf{A}_1 \mathbf{y} + \mathbf{a}_1) - \mathbf{v}_1^* \leq 0,$$

where $\mathbf{Z}_r \in \mathbb{R}^{(2n+6+6c)\times z_r}$ represents a surjective mapping into the nullspace of all previous equalities $\mathbf{W}_r\mathbf{B}_r, \ldots, \mathbf{W}_1\mathbf{B}_1$ and $\mathbf{u}_r \in \mathbb{R}^{z_r}$ is a variable that parameterizes that nullspace. In order to compute $\mathbf{Z}_r$ a Singular Value Decomposition (SVD) can be performed. In our case it is performed in parallel with the QP at priority level $r-1$ and rarely finishes after the QP, such that it adds only a negligable overhead. Now, we can express a QP of the next lower priority level $r+1$ and additionally impose the constraints in Eqs. (8),(9), s.t. we can optimize over $\mathbf{y}$ without violating optimality of higher priority QPs:

$$\min_{\mathbf{u}_{r+1}, \mathbf{v}_{r+1}} \quad \|\mathbf{v}_{r+1}\| + \|\mathbf{W}_{r+1}(\mathbf{B}_{r+1}(\mathbf{y}_r^* + \mathbf{Z}_r\mathbf{u}_{r+1}) + \mathbf{b}_{r+1})\| \tag{10}$$

s.t.

$$\mathbf{V}_{r+1}(\mathbf{A}_{r+1}(\mathbf{y}_r^* + \mathbf{Z}_r\mathbf{u}_{r+1},) + \mathbf{a}_{r+1}) \leq \mathbf{v}_{r+1},$$
$$\mathbf{V}_r(\mathbf{A}_r(\mathbf{y}_r^* + \mathbf{Z}_r\mathbf{u}_{r+1},) + \mathbf{a}_r) \leq \mathbf{v}_r^*, \tag{11}$$
$$\vdots$$
$$\mathbf{V}_1(\mathbf{A}_1(\mathbf{y}_r^* + \mathbf{Z}_r\mathbf{u}_{r+1},) + \mathbf{a}_1) \leq \mathbf{v}_1^*,$$

where we wrote the QP as in Eq. (5) and substituted $\mathbf{w}$ into the objective function. In order to ensure that we optimize over the optimal solutions of higher priority tasks, we added Eq. (9) as an additional constraint and substituted Eq (8) into Eqs. (10)-(11). This allows us to solve a stack of hierarchical tasks recursively as originally proposed by [13]. Note that this optimization algorithm is guaranteed to find the optimal solution in a least-squares sense while satisfying priorities.

C. Decomposition of Equations of Motion

Hierarchical inverse dynamics approaches usually have in common that consistency of the variables with physics, i.e. the equations of motion, need to be ensured. In [13] these constraints are expressed as equality constraints (with slacks) resulting in an optimization problem over all variables $\ddot{\mathbf{q}}, \boldsymbol{\tau}, \boldsymbol{\lambda}$. In [14] a mapping into the nullspace of Eq. (1) is optained from a SVD on Eq. (1). In both cases complexity can be reduced as we will show in the following. We decompose the equations of motion as

$$\mathbf{M_u}(\mathbf{q})\ddot{\mathbf{q}} + \mathbf{N_u}(\mathbf{q}, \dot{\mathbf{q}}) = \boldsymbol{\tau} + \mathbf{J}_{c,u}^T\boldsymbol{\lambda}, \tag{12}$$
$$\mathbf{M_l}(\mathbf{q})\ddot{\mathbf{q}} + \mathbf{N_l}(\mathbf{q}, \dot{\mathbf{q}}) = \mathbf{J}_{c,l}^T\boldsymbol{\lambda} \tag{13}$$

where Eq. (12) is just the first n equations of Eq. (1) and eq. (13) is the last 6 equations related to the floating base. The latter can then be interpreted as the Newton-Euler equations of the whole system [16]. They express the change of momentum of the robot as a function of external forces.

Fig. 1. The lower part of the Sarcos Humanoid on which experiments were conducted. Credit: Luke Fisher Photography.

A remarkable feature of the decomposition in Eqs. (12), (13) is that the torques $\boldsymbol{\tau}$ only occur in Eq. (12) and are exactly determined by $\ddot{\mathbf{q}}, \boldsymbol{\lambda}$ in the form

$$\boldsymbol{\tau} = \mathbf{M_u}(\mathbf{q})\ddot{\mathbf{q}} + \mathbf{N_u}(\mathbf{q}, \dot{\mathbf{q}}) - \mathbf{J}_{c,u}^T\boldsymbol{\lambda} \tag{14}$$

Since $\boldsymbol{\tau}$ is linearly dependent on $\ddot{\mathbf{q}}, \boldsymbol{\lambda}$, for any combination of accelerations and contact forces there always exist a solution for $\boldsymbol{\tau}$. It is given by Eq. (12). Therefore, it is only necessary to use Eq. (13) as a constraint for the equations of motion during the optimization (i.e. the evolution of momentum is the only constraint).

Because of the linear dependence, all occurrences of $\boldsymbol{\tau}$ in the problem formulation (i.e. in Eqs. (3)-(4)) can be substituted by Eq. (14). This reduces the number of variables in the optimization from $(2n + 6 + 6c)$ to $(n + 6 + 6c)$. This decomposition thus saves as many variables as there are DoFs on the robot. Such simplification was crucial for us to reduce the time taken by the optimizer and allowed us to implement the controller in a 1KHz feedback control loop.

III. EXPERIMENTAL SETUP

We now explain the experimental setup and its limitations.

A. Sarcos Humanoid Robot

The experiments were done on the lower part of the Sarcos Humanoid Robot [2] (Fig. 1). It consists of two legs and a torso. The legs have 7 DOFs each and the torso has 3 DOFs. Given that the torso supports a negligible mass because it is not connected to the upper body of the robot and its motion does not change much the dynamics, we froze these DOFs during the experiments. The legs of the robot are 0.82m high. Each foot is 0.09m wide and 0.25m long, which is rather small for a biped. Note also that the front of the foot is made of a passive joint that is rather stiff, located 10cm before the tip of the foot. The total robot mass is 51kg. The robot is actuated with hydraulics and each joint consists of a Moog Series 30 flow control servo valve with a piston on which

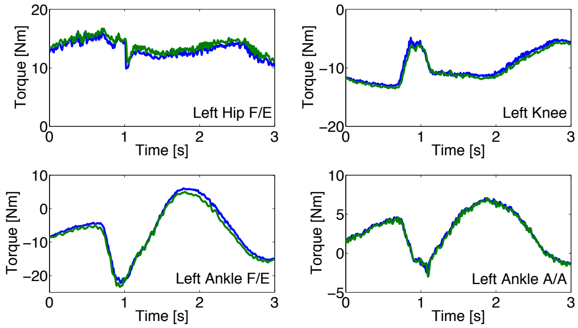

Fig. 2. Example of torque tracking performance during a balancing experiment. The left hip flexion/extension, left knee and left ankle flexion/extension and adduction/abduction joints are shown. Both desired (blue) and actual (green) torques are shown.

a load cell is attached to measure the force at the piston. A position sensor is also located at the joint. Each foot has a 6-axis force sensor and we mounted an IMU on the pelvis of the robot from which we measure angular velocities, linear accelerations and the orientation of the robot in an inertial frame. An offboard computer sends control commands to the robot at 1KHz. The control commands consist of the desired current applied to each valve.

B. Low-level torque control

For each actuator, we implemented a torque feedback controller that ensures that each joint produces the desired force generated by the balance controller. The controller essentially computes desired valve commands given a desired torque, the valve commands representing a desired flow. The controller we implemented is very much inspired from the work in [3], [17], with the difference that we implemented a simpler version where piston velocity feedback has a constant gain. The control law is

$$v = PID(F_{des}, F) + K\dot{x}_{piston} + d \tag{15}$$

where v is the valve command, PID is a PID control according to desired force command and force measured from the load cells, K is a positive gain, $\dot{x}_{piston}$ is the piston velocity (computed from the joint velocity) and d is a constant bias.

This controller design allowed us to achieve good torque tracking performance. It is important to note that it was necessary to achieve good performance in the hierarchical inverse dynamics controller. Figure 2 illustrates the torque tracking performance during the balancing experiment.

C. Limitations

During the experiments, we suffered from two important limitations. First, our dynamic model is based on the CAD model of the robot. It means that it is not very accurate as it does not take into account the contribution of the hydraulic hoses, the electronics nor any type of friction in the model. Second, we relied on very simple state estimation from the floating base. We just integrated the acceleration readings to get the base velocity and position, using a decay term to damp velocities.

However, these limitations are not too problematic as we show in the experiments. Furthermore, they can be overcome by using system identification [18] and filtering [19] methods that have proven to work well on legged robots.

IV. EXPERIMENTS

We formulated balancing and motion tracking tasks in the framework discussed in Sect. II and evaluated them on the Sarcos Humanoid described in Sect. III. The performance of the robot was tested in two different scenarios: a balancing task and a tracking task. A summary of the experiments is shown in the attached movie [1].

For all the experiments, we run the hierarchical inverse dynamics controller as a feedback controller that computes directly the desired torque commands. We do not use any joint PD controller for stabilization and the feedback is computed purely in task space.

A. Processing Time

First, we had to make sure that the controller was fast enough to run in the 1KHz control loop. We also compared the gain in speed with the simplification proposed in Section II-C.

Priority	Nr. of eq(uality) and ineq(uality) constraints	Constraint/Task
1	25 eq	Eq. (12) (not required for simplified problem)
	6 eq	Newton Euler Eq. (13)
	2×25 ineq	torque limits
2	$c \times 6$ eq	kinematic contact constraint
	$c \times 4$ ineq	CoPs reside in support polygons
	$c \times 4$ ineq	GRFs reside in friction cones
	2×25 ineq	joint acceleration limits
3	3 eq	PD control on CoM
	$(2-c) \times 6$	PD control on swing foot
4	$25 + 6$ eq	PD control on posture
5	$c \times 6$ eq	regularizer on GRFs

TABLE I

STEPPING TASK FOR FULL HUMANOID FOR COMPARISON OF COMPUTATION TIME

The tests were done on an Intel Core i7-2600 CPU with 3.40GHz. A stepping task was designed for a 25 DoFs humanoid robot to run in simulation as summarized in Table I. The problem size changed dependent on the number of contacts c ($c = 2$ in double support and $c = 1$ in single support). The proposed decomposition removed 25 equality constraints and 25 optimization variables. We measured the computation time of both versions of the hierarchical solver, one with the full EoM and one with the proposed reduction. The computation time at each control cycle is plotted in Fig. 3. Looking at the worst case (as this is significant for execution in a time critical control loop) we can drop computation time by 40%. This allows us to run a 1kHz

[1]An extended version is also available on http://youtu.be/jCi-VkctmY4

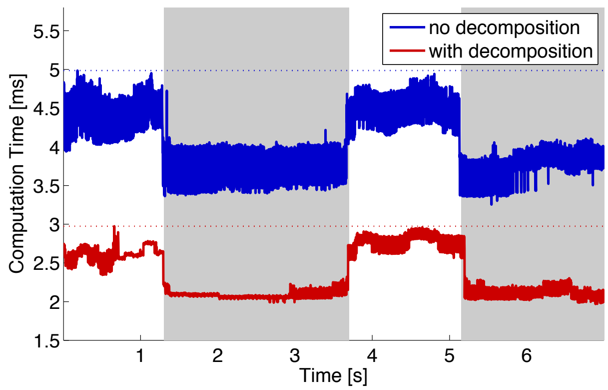

Fig. 3. Processing time of a stepping task using the decomposition proposed in Sect. II-C (red) and the same task performed without the decomposition (blue). The dotted line represents the maximum computation per control cycle respectively. Intervals shaded in gray show the robot in single support phase. In the remaining time the robot is in double support. With the proposed decomposition we decreased the computation time by approximately 40%.

control-loop on a 14 DoF robot as we will demonstrate in the following sections. It would not have been possible with our solver without the simplification. In our speed comparison in Fig. 3 one can see that computation time varies with the number of constrained endeffectors, which can be problematic if the number of contacts increases too much (e.g. when using both hands and feet).

B. Balance Control Experiments

Our first experiment is the implementation of a momentum balance controller as originally proposed in [15] and then extend in [11]. The idea is to regulate both the linear and angular momentum of the robot to keep balance. In this implementation, the physical constraints are put in the highest priority. In the second priority, we put the balancing task as well as the force regularization and postural control. The tasks used are summarized in Table II.

In [20] a linear mapping

$$\mathbf{H_G}(\mathbf{q})\dot{\mathbf{q}} = \mathbf{h} \tag{16}$$

was derived that maps joint velocities to $\mathbf{h}^T = [\mathbf{h}_{lin}^T \ \mathbf{h}_{ang}^T]$, the system linear and angular momentum expressed at the CoM. The matrix $\mathbf{H_G}$ is called the centroidal momentum matrix. It was applied in [11] to regulate the momentum by computing a desired momentum rate of change via PD control

$$\begin{aligned}\dot{\mathbf{h}}_{ref} &= \mathbf{P}\begin{bmatrix} m(\mathbf{x}_{cog,des} - \mathbf{x}_{cog}) \\ \mathbf{0} \end{bmatrix} + \\ &\quad \mathbf{D}(\mathbf{h}_{des} - \mathbf{h}) + \dot{\mathbf{h}}_{des} \end{aligned} \tag{17}$$

where $\mathbf{P}$ and $\mathbf{D}$ are positive-definite gain matrices. Typically, this can be used to regulate the position of the center of mass while damping its linear velocity and the angular momentum. The derivative of Eq. (16) allows us to express a controller

Priority	Nr. of eq(uality) and ineq(uality) constraints	Constraint/Task
1	6 eq	Newton Euler Eq. (13)
	2×14 ineq	torque limits
	2×6 eq	kinematic contact constraint
	2×4 ineq	CoPs reside in support polygons
	2×4 ineq	GRFs reside in friction cones
	2×14 ineq	joint acceleration limits
2	6 eq	PD control on system momentum, Eq. (17)
	$14 + 6$ eq	PD control on posture
	2×6 eq	regularizer on GRFs

TABLE II
HIERARCHY OF TASKS USED IN THE BALANCE EXPERIMENT

on the system momentum

$$\dot{\mathbf{h}} = \mathbf{H_G}\ddot{\mathbf{q}} + \dot{\mathbf{H}}_\mathbf{G}\dot{\mathbf{q}} \tag{18}$$

$$= \begin{bmatrix} \mathbf{I}_{3\times3} & \mathbf{0}_{3\times3} & \dots \\ [\mathbf{x}_{cog} - \mathbf{x}_i]_\times & \mathbf{I}_{3\times3} & \dots \end{bmatrix} \boldsymbol{\lambda} + \begin{bmatrix} m\mathbf{g} \\ \mathbf{0}, \end{bmatrix} \tag{19}$$

where $m\mathbf{g}$ is the gravitational force applied at the CoM and $[\boldsymbol{\cdot}]_\times$ maps a vector to a skew symmetric matrix, s.t. $[\mathbf{x}]_\times \boldsymbol{\lambda} = \mathbf{x} \times \boldsymbol{\lambda}$. Eq. (19) is the general formula for the *change of momentum* of a rigid multi-body system. We see that we can express the rate of momentum change either as a function of $\ddot{\mathbf{q}}$ as in Eq. (18) or as a function of $\boldsymbol{\lambda}$ as in Eq. (19). We can express this task either as a force task or as a kinematic task (the matrix in front of $\ddot{\mathbf{q}}$ or $\boldsymbol{\lambda}$ being the Jacobian of the task). In this experiment we use the kinematic representation and in the tracking experiment we use the force representation. We note that in general, expressing the momentum control with Eq. (19) might be better because we do not have to compute $\dot{\mathbf{H}}_G$, which usually is acquired through numerical derivation and might suffer from magnified noise.

In our first experiment we pushed the robot impulsively with a stick. Various contact points and force directions were chosen. To ensure that the robot is really balancing, the same experiment was conducted when running a simple inverse dynamics algorithm with contact forces optimization that was presented in [8]. As expected, the balance controller showed a better balancing performance and did not fall over as it was the case for [8] as can be seen in the video. When pushing the robot with a constant force at various parts, it stayed in balance and adapted its positions in a compliant manner. We also tested the controller when the feet were not co-planar, but one foot was put on top of a block as can be seen on the movie.

In the planar posture, even pushes with a rather high magnitude were absorbed and the robot kept standing. The change in momentum was damped out quickly and the CoM was tracked after an initial disturbance as can be seen in Fig. 4. The CoPs remained inside of the support polygons and were tracked well. We notice from Figure 4 that the CoP predictions are approximately correct (within 2cm error). However, one can expect that a higher precision might be needed to achieve dynamic motions which could be achieved with an inertial parameters estimation procedure [18].

Priority	Nr. of eq(uality) and ineq(uality) constraints	Constraint/Task
1	6 eq	Newton Euler Eq. (13)
	2×14 ineq	torque limits
2	2×6 eq	kinematic contact constraint
	2×4 ineq	CoPs reside in support polygons
	2×4 ineq	GRFs reside in friction cones
	2×14 ineq	joint acceleration limits
3	3 eq	PD control on CoG
4	$14 + 6$ eq	PD control on posture
5	2×6 eq	regularizer on GRFs

TABLE III

HIERARCHY OF TASKS USED IN THE TRACKING EXPERIMENT

For our next experiment we put the biped on a rolling platform and rotated and moved it with a rather fast change of directions. Although, the CoM was moving away from its desired position initially, the momentum change was damped out and the robot kept standing and recovered CoM tracking. The stationary feet indicated that forces were applied that were consistent with our CoP boundaries.

In an additional scenario the biped was standing on a balancing board. We ran the experiment with two configurations for the robot: in one case the robot is standing such that the board motion happens in the sagittal plane and in the other case the motion happens in the lateral plane. Figure 5 shows results when the motion happens in the lateral plane. In this case, the slope was varied in a range of $[-9.5°; 9.5°]$. Even for quite rapid changes in the slope, the feet remained flat on the ground. Compared to the push experiment the CoPs were moving in a wider range, but still remained in the interior of the foot soles with a margin. In this case, we notice a discrepancy in the predicted contact forces and the real ones, making the case for a better dynamics model. Yet, the robot was still able to balance.

When we increased the pushes on the robot, eventually the momentum could not be damped out fast enough anymore and the robot reached a situation where the optimization could not find solutions anymore and the biped fell. In these cases the constraint that the feet have to be stationary was too restrictive. A higher level controller that takes into account stepping [21], [22] becomes necessary to increase the stability margin. It took approximately 0.4ms to solve the optimization problem at each control cycle. This is already fast enough for the 1KHz control loop of the robot.

C. Tracking Experiments

We also performed a tracking experiment. The goal was to track a desired CoM motion while satisfying the physical constraints. The lower priority tasks consist of joint posture tracking and contact forces regularization (i.e. we minimize tangential contact forces). We wrote the CoM tracking task as a force task, using Eq. (19) where the desired CoM acceleration is computed using a PD controller. The full hierarchy of tasks used in this experiment is shown in Table III.

The CoM performed various sine wave tracking tasks. The

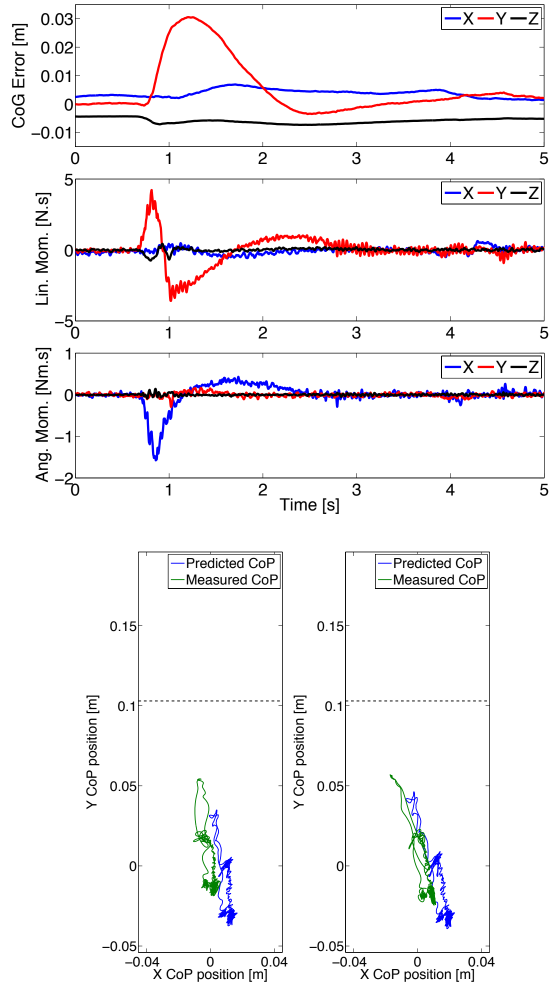

Fig. 4. This figure shows the recovery of desired CoG position, linear and angular momentum after a push from the front. X points in the robot right direction, Y in the forward direction and Z in the vertical direction. The change in CoP for each leg is also plotted in the lower graph. The plot has the same ratio than the feet and the horizontal dashed line shows the position of the passive joint at the front of the foot.

first one was a 0.3Hz sine wave with 0.02m amplitude in the forward direction and 0.03m in the vertical direction. The second one was a larger amplitude (0.06m) sine wave only in the vertical direction. Figure 6 shows the typical tracking performance during these tasks. During the tracking experiments the robot was still able to handle a certain level of disturbances, as can be seen in the attached video but not as much as when the angular momentum was also regulated.

In this experiment we use much more hierarchies than in the previous one. In this case, the controller was able to compute the control commands in an average of 0.9ms (standard deviation of 0.045). We see that in the current state, the hierarchical inverse dynamics is at the limit of the number of hierarchies it can solve in the 1KHz control cycle.

V. DISCUSSION

In the following we discuss the results we presented and how they relate to other approaches.

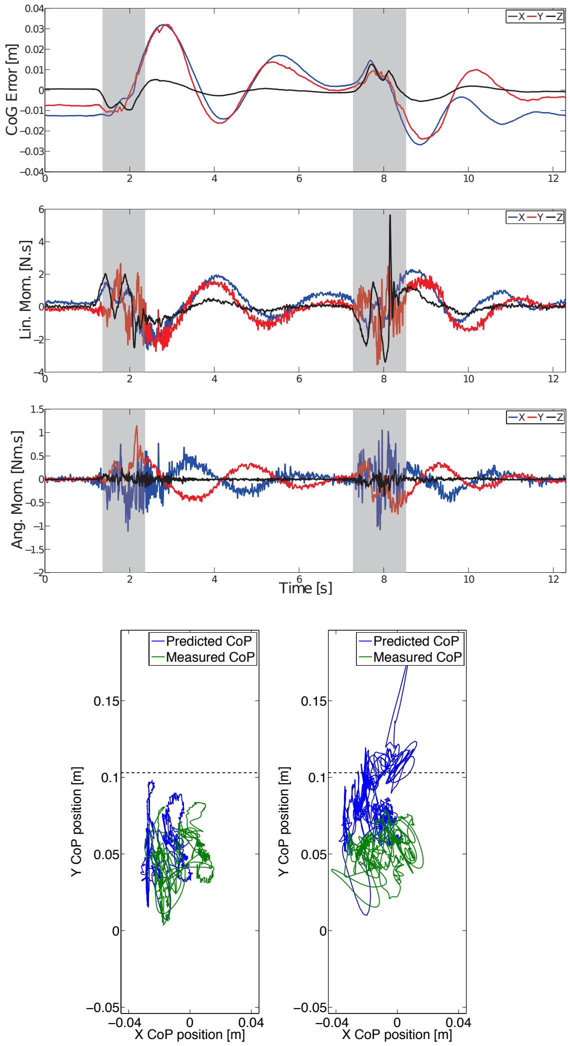

Fig. 5. This figure shows the recovery of desired CoG position, linear and angular momentum during the balance board experiment. X points in the robot right direction, Y in the forward direction and Z in the vertical direction. The grey shades are the moments when the board is moving, first up, then down. The total angle motion is from $-9.5°$ to $9.5°$ with respect to horizontal.

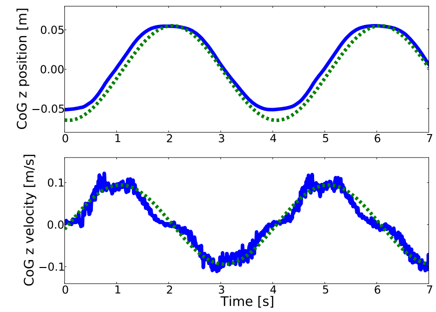

(a) 0.25 Hz high amplitude tracking task

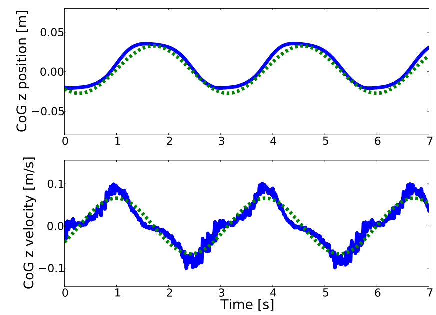

(b) 0.3 Hz low amplitude tracking task

Fig. 6. Plot of the vertical CoM tracking performance for two tracking tasks. Both the positions (upper graphs) and velocities (lower graph) are shown in the plots. We note that both the desired positions and velocities (green dashed line) match very well the actual (blue plain line). The position RMSE is 0.0094m for the upper plot and 0.0058 for the lower plot.

A. Relation to other balancing approaches

The balance controller presented in the first experiment is a slight reformulation of the momentum-based controller presented by Lee and Goswami [11], [23]. Our formulation has the great advantage to solve a single optimization problem instead of several ones and can therefore guarantee that the control law will be consistent with all the constraints (joint limits, accelerations, torque saturation, CoP limits and contact force limitations). Furthermore, we search over the full set of possible solutions and thus we are guaranteed to find the optimum, where [11], [23] optimize over sub-parts of the variables sequentially. It is also different from the work of [15] because we explicitly take into account contact forces in the optimization and not purely kinematics.

The balance controller is very much related to the work of Stephens et al. [12]. In [12], the authors write the whole optimization procedure using Eq. (1) with constraints similar to what we have. However, the optimization problem being complicated, they actually solve a simpler problem were the contact forces are first determined and then desired accelerations and torques are computed through a least-square solution. From that point of view, torque saturation and limits on accelerations are not accounted for. In our experiments, no tradeoff is necessary and we solve for all the constraints exactly. Further, we can introduce more hierarchies and thus do strict separation of constraints and tasks as demonstrated in the experiments.

B. Relations with other hierarchical inverse dynamics solvers

In the hierarchical task solver that was used in this paper, we exploited the fact that the null space mapping of one priority could be computed in parallel with solving the QP of the same priority. However, a drawback is that inequality constraints from higher priorities have to be carried through all lower priority QPs. The algorithm presented in [14] solves only one QP with all inequality constraints included once. However, the null spaces are computed in advance in order to formulate the QP. It is not clear which approach would be more efficient and a speed comparison would be very interesting. Their approach can also profit from the decomposition proposed in this paper, then it will not be required to compute an SVD of the full equations of motion, but only of the last six rows.

Some improvements can also be done on the QP solver that we use. For example, we solve each QP without considering the previous solutions. It is very inefficient since the control commands are likely to be very close to each other between each control cycle. Implementing a sort of warm start that takes into account the previous solution and the active sets could decrease significantly the computational time. Such improvements will be necessary in order to handle more contacts and a larger number of DOFs.

VI. CONCLUSION

In this paper we have presented experimental results using a hierarchical inverse dynamics controller. To the best of our knowledge, it is the first implementation of such an approach on a torque controlled humanoid robot in a fast control loop. We have presented both balance and tracking experiments. Our results suggest that the use of complete dynamic models and hierarchies of tasks for feedback control is a feasible approach, despite the model inaccuracies and computational complexity.

ACKNOWLEDGMENT

We would like to thank Ambarish Goswami and Seungkook Yun for hosting us at the Honda Research Institute for one week and for their precious help in understanding the original momentum-based controller. We would also like to thank Ambarish Goswami and Sung-Hee Lee for giving us an early access to their publication. We are also grateful to Daniel Kappler for helping us with the videos, Nick Rotella for helping with the data acquisition from the IMU and Sean Mason for the help with the inertial parameters of the robot.

REFERENCES

[1] M. Hutter, M. A. Hoepflinger, C. Gehring, M. Bloesch, C. D. Remy, and R. Siegwart, "Hybrid Operational Space Control for Compliant Legged Systems," in *Robotics: Science and Systems (R:SS)*, 2012.

[2] G. Cheng, H. Sang-Ho, A. Ude, J. Morimoto, J. G. Hale, J. Hart, J. Nakanishi, D. Bentivegna, J. Hodgins, C. Atkeson, M. Mistry, S. Schaal, and M. Kawato, "CB: Exploring Neuroscience with a Humanoid Research Platform," in *IEEE Intl Conf on Robotics and Automation*, 2008, pp. 1772–1773.

[3] T. Boaventura, C. Semini, J. Buchli, M. Frigerio, M. Focchi, and D. Caldwell, "Dynamic Torque Control of a Hydraulic Quadruped Robot," in *IEEE Intl Conf on Robotics and Automation*, 2012, pp. 1–6.

[4] C. Ott, M. A. Roa, and G. Hirzinger, "Posture and balance control for biped robots based on contact force optimization," in *IEEE-RAS Intl Conf on Humanoid Robots*, 2011.

[5] M. Kalakrishnan, J. Buchli, P. Pastor, M. Mistry, and S. Schaal, "Learning, Planning, and Control for Quadruped Locomotion over Challenging Terrain," *The Intl Journal of Robotics Research*, vol. 30, no. 2, pp. 236–258, 2011.

[6] L. Saab, O. Ramos, N. Mansard, P. Soueres, and J.-Y. Fourquet, "Generic Dynamic Motion Generation with Multiple Unilateral Constraints," in *IEEE/RSJ Intl Conf on Intelligent Robots and Systems*, 2011, pp. 4127–4133.

[7] J. Salini, V. Padois, and P. Bidaud, "Synthesis of Complex Humanoid Whole-Body Behavior: A Focus on Sequencing and Tasks Transitions," in *IEEE Intl Conf on Robotics and Automation*, 2011, pp. 1283–1290.

[8] L. Righetti and S. Schaal, "Quadratic programming for inverse dynamics with optimal distribution of contact forces," in *IEEE-RAS Intl Conf on Humanoid Robots*, 2012, pp. 538–543.

[9] L. Righetti, J. Buchli, M. Mistry, M. Kalakrishnan, and S. Schaal, "Optimal distribution of contact forces with inverse-dynamics control," *The Intl Journal of Robotics Research*, vol. 32, no. 3, pp. 280–298, 2013.

[10] S.-H. Hyon, J. G. Hale, and G. Cheng, "Full-Body Compliant Human–Humanoid Interaction: Balancing in the Presence of Unknown External Forces," *IEEE Transactions on Robotics*, vol. 23, no. 5, pp. 884–898, 2007.

[11] S.-H. Lee and A. Goswami, "A momentum-based balance controller for humanoid robots on non-level and non-stationary ground," *Autonomous Robots*, vol. 33, pp. 399–414, 2012.

[12] B. J. Stephens and C. G. Atkeson, "Dynamic Balance Force Control for compliant humanoid robots," in *IEEE/RSJ Intl Conf on Intelligent Robots and Systems*, 2010, pp. 1248–1255.

[13] M. de Lasa, I. Mordatch, and A. Hertzmann, "Feature-Based Locomotion Controllers," *ACM Transactions on Graphics*, vol. 29, no. 3, 2010.

[14] N. Mansard, "A dedicated solver for fast operational-space inverse dynamics," in *Robotics and Automation (ICRA), 2012 IEEE International Conference on*, 2012, pp. 4943–4949.

[15] S. Kajita, F. Kanehiro, K. Kaneko, K. Fujiwara, K. Harada, K. Yokoi, and H. Hirukawa, "Resolved momentum control: humanoid motion planning based on the linear and angular momentum," in *Intelligent Robots and Systems, 2003. (IROS 2003). Proceedings. 2003 IEEE/RSJ International Conference on*, 2003, pp. 1644–1650.

[16] P. Wieber, "Holonomy and nonholonomy in the dynamics of articulated motion," *Fast motions in biomechanics and robotics*, pp. 411–425, 2006.

[17] T. Boaventura, M. Focchi, M. Frigerio, J. Buchli, C. Semini, G. A. Medrano-Cerda, and D. Caldwell, "On the role of load motion compensation in high-performance force control," in *IEEE/RSJ Intl Conf on Intelligent Robots and Systems*, 2012, pp. 4066–4071.

[18] M. Mistry, S. Schaal, and K. Yamane, "Inertial Parameter Estimation of Floating Base Humanoid Systems using Partial Force Sensing," in *IEEE-RAS Intl Conf on Humanoid Robots*, 2009, pp. 492–497.

[19] M. Bloesch, M. Hutter, M. H. Hoepflinger, C. D. Remy, C. Gehring, and R. Siegwart, "State estimation for legged robots-consistent fusion of leg kinematics and IMU," in *Robotics: Science and Systems (R:SS)*, 2012.

[20] D. E. Orin and A. Goswami, "Centroidal Momentum Matrix of a humanoid robot: Structure and Properties," in *IEEE/RSJ Intl Conf on Intelligent Robots and Systems*, 2008, pp. 653–659.

[21] J. Pratt, T. Koolen, T. De Boer, J. Rebula, S. Cotton, J. Carff, M. Johnson, and P. Neuhaus, "Capturability-based analysis and control of legged locomotion, Part 2: Application to M2V2, a lower-body humanoid," *The Intl Journal of Robotics Research*, vol. 31, no. 10, 2012.

[22] J. Urata, K. Nshiwaki, Y. Nakanishi, K. Okada, S. Kagami, and M. Inaba, "Online Walking Pattern Generation for Push Recovery and Minimum Delay to Commanded Change of Direction and Speed," in *IEEE/RSJ Intl Conf on Intelligent Robots and Systems*, 2012, pp. 3411–3416.

[23] S.-H. Lee and A. Goswami, "Ground reaction force control at each foot: A momentum-based humanoid balance controller for non-level and non-stationary ground," in *IEEE/RSJ Intl Conf on Intelligent Robots and Systems*, 2010, pp. 3157–3162.